Insights into the potential functions of nucleoside diphosphate kinases in *Waddlia chondrophila* encoded by two *ndk* paralogs

Giti Ghazi-Soltani, Carole Kebbi-Beghdadi, Simone E. Adams, Gilbert Greub*

Center for Research on Intracellular Bacteria, Institute of Microbiology, University Hospital Center and University of Lausanne, Lausanne, Switzerland

* Corresponding author:
Prof. Gilbert Greub: gilbert.greub@chuv.ch

ABSTRACT

The *Chlamydiota* phylum consists of obligate intracellular bacteria, including well-known pathogens and emerging environmental species, with diverse host ranges and metabolic capabilities. Among these bacteria, the *ndk* gene, which encodes nucleoside diphosphate kinase, is present in variable copy numbers. While most chlamydial species carry a single copy of the *ndk* gene, some species have two copies. In *W. chondrophila*, both *ndk* paralogs retain conserved kinase motifs but differ in subcellular localization, suggesting divergent functional roles. *WcNdk1* is confined to the inclusion and likely supports nucleotide metabolism, while *WcNdk2* localizes to the host nucleus, perinuclear space, and Golgi apparatus, implying involvement in host interaction. Azidothymidine (AZT), a known Ndk inhibitor, was found to impair the growth of *W. chondrophila*, possibly by targeting WcNdk2 due to its role in host interaction. Our findings shed light on the potential functions of *ndk* paralogs in *W. chondrophila* and support a role for WcNdk2 in host manipulation and pathogenesis. This research offers a starting point for deeper functional analyses as genetic manipulation techniques for this organism become more accessible.

Keywords: *Waddlia chondrophila*, Nucleoside diphosphate kinase (Ndk), AZT inhibition, Subcellular localization, Protein trafficking

INTRODUCTION

The *Chlamydiota* phylum encompasses several families of obligate intracellular bacteria, including five main families beyond the well-known *Chlamydiaceae*: *Parachlamydiaceae*, *Waddliaceae*, *Simkaniaceae*, *Rhabdochlamydiaceae*, and *Criblamydiaceae*. Members of these families share a chlamydia-like developmental cycle, which reflects their adaptation to intracellular environments and reliance on host cell machinery for survival.

W. chondrophila belongs to the family *Waddliaceae* and is known as an abortigenic agent in ruminants. It was first isolated from aborted bovine fetus[1,2] and serological studies showed a strong association between anti-*Waddlia* antibodies and bovine abortion[3]. In humans, *W. chondrophila* seropositivity is significantly associated with adverse pregnancy outcomes[4–6]. This pathogen was also detected in respiratory tract samples of patients with pneumonia and children with bronchiolitis[7,8].

The *W. chondrophila* developmental cycle is biphasic and is divided into three major phases[9,10]. In the early phase (0-8 hours post-infection, hpi) elementary bodies (EBs) enter in host cells and differentiate into reticulate bodies (RBs). This phase is followed by a proliferation phase (8-24 hpi) during which the number of RBs increases exponentially through binary fission. In the late phase (24-48 hpi) RBs revert into EBs which lyse the host cell to release infectious progeny. Under environmental or antibiotic stress, the developmental cycle is arrested and this leads into an enlarged, non-dividing RB-like form called Aberrant Body (AB)[11]. While *W. chondrophila* significantly impacts both animal and human health, the specific molecular and genomic pathways, particularly those involving developmental and regulatory proteins, remain largely unexplored. Functional characterization of proteins, such as nucleoside diphosphate kinase (Ndk), could help us to better understand the biology and pathogenicity of this pathogen and its adaptation inside host cells.

Ndk is a highly conserved enzyme that plays a central role in maintaining nucleotide pools. The maintenance of intracellular NTP pools is vital for the survival and proliferation of all living organisms. Ndk regulates nucleotide pools through its autophosphorylation and phosphotransferase activities. This ensures that NTP and dNTP levels remain balanced for optimal cellular function.

Beyond its housekeeping functions, Ndk is implicated in various cellular processes, including cell differentiation and development in eukaryotes and prokaryotes[12–15]. Additionally, Ndk is involved in the regulation of gene expression[16–18]. Due to its ability to bind ATP, Ndk is

62 involved in inhibiting extracellular ATP (eATP) and disrupting purinergic signaling in immune
63 and inflammatory responses[19–21].
64 We previously reported *W. chondrophila* transcriptomic data comparing genes expression in
65 RBs (24h pi) and EBs (72h pi)[22]. In this study *ndk* was among the genes differentially expressed
66 between the two developmental stages. Despite the well-established functions of Ndk across
67 various organisms, its specific function in the *Chlamydiae* remains uncharacterized. Based on
68 these observations, we hypothesized that this enzyme could play an important role in the
69 development and pathogenesis of *Chlamydia*-like organism. In this study, we characterize the
70 two Ndk proteins in *W. chondrophila* to better understand their potential role in the bacterium's
71 development and pathogenicity. This study provides an overall view of Ndk proteins in the
72 *Chlamydiota* phylum and offers a foundational characterization of *W. chondrophila* Ndks. Our
73 results pave the way for more detailed research once genetic tools become available for *W.*
74 *chondrophila*.

75 RESULTS

76 **Evolution of the *ndk* operon in the *Chlamydiota* phylum**
77 Similar to other organisms, bacteria of the *Chlamydiota* phylum possess at least one copy of
78 the *ndk* gene. A second copy (*ndk2*) is present in members of the *Parachlamydiaceae*,
79 *Waddliaceae*, and *Criblamydiaceae* families (Figure 1A). Interestingly, another *ndk2* forms an
80 operon with the ancestral *ndk1* gene. This operon in majority of species is further associated
81 with *pabA*, which encodes para-aminobenzoate synthase, and is involved in the folate
82 biosynthesis pathway. Comparisons of gene-based and species-based phylogenetic trees
83 (Figure 1B and 1C) suggest that the duplication of *ndk2* most likely originated from a single
84 duplication in the common ancestor of *Parachlamydiaceae*, *Waddliaceae*, and
85 *Criblamydiaceae*; however, a scenario of ancestral duplication with subsequent loss in
86 *Simkaniaceae* and *Chlamydiaceae* cannot be excluded, though it is less parsimonious.

87 **High sequence and structural conservation of Ndk across species**
88 The multiple sequence alignment shows a high degree of sequence conservation of Ndk
89 proteins from various bacterial and eukaryotic species (Figure 2A). Specifically, the His-Gly-
90 Ser-Asp (HGSD) motif, which is the enzyme's active site[23], is well conserved across all aligned
91 sequences. The highly conserved histidine residue inside this motif transiently receives the
92 phosphate group during autophosphorylation reaction and is, therefore, critical for the catalytic
93 function of Ndk. In addition to the HGSD motif, other conserved residues are observed in

94 regions associated with nucleotide binding and structural stability, many of which are enriched
95 in hydrophobic amino acids. These residues likely contribute to the proper folding and
96 enzymatic efficiency of Ndk.
97 *W. chondrophila* contains two copies of *ndk*: *wcndk1 (*locus *wcw_1543*) and *wcndk2* (locus
98 *wcw_1545*), with a sequence similarity of 54% (Figure 2B). The most striking difference
99 between the two *W. chondrophila ndk* paralogs is the presence of a predicted signal peptide of
100 17 amino acids in WcNdk2, which is absent in WcNdk1.
101 The sequence similarity matrix of *W. chondrophila* Ndk proteins, WcNdk1 and WcNdk2, and
102 their counterparts from other bacterial and eukaryotic species shows differing degrees of
103 conservation as shown in Figure 2B. WcNdk1 shares the highest sequence identity with *E. coli*
104 Ndk (EcNdk) and *Chlamydia trachomatis* Ndk (CtNdk) (67 % and 66%, respectively). In
105 contrast, WcNdk2 exhibits slightly lower sequence similarity across species, which may
106 indicate functional divergence of the two Ndks following gene duplication. Interestingly, both
107 *W. chondrophila* Ndk homologs display relatively high sequence identity (~50%) with human
108 Ndk (HsNdk), which suggests the conservation of core functional domains across vast
109 evolutionary distance. Sequence similarity matrix of Ndk proteins across different species is
110 shown in Figure S2.
111 WcNdk1 has 143 residues forming a polypeptide chain and adopting a very similar fold to Ndk
112 protein from other origins including human Ndk[24,25] (Figure 2C). One Ndk unit has α/β
113 domains comprising a four-stranded antiparallel β-sheet and two connecting α-helices. This
114 high degree of sequence and structural conservation between eukaryotes and the pathogens
115 may enable them to interfere with host cellular process by mimicking host Ndk.

116 **Expression profile of *W. chondrophila* Ndks during infection**

117 Temporal expression levels of gene and protein across different developmental stages may help
118 us understand their stage-specific roles and regulatory mechanisms. Since each of these phases
119 has unique biological features, we can infer a protein's function by mapping both transcript
120 and protein levels across these stages.
121 We quantified the expression profiles of *W. chondrophila ndks*, at both the transcript and
122 protein level during host cell infection (Figure 3). *wcndk1* and *wcndk2* transcripts were highly
123 abundant at early time points (3-8 hpi) as revealed by RT-qPCR, then the mRNA level declined
124 sharply to a minimum at 32 hpi, with a moderate surge toward the end of the cycle (48 hpi),
125 (Figure 3A). In parallel, no WcNdk1 or WcNdk2 protein could be detected by western blot of
126 the *W. chondrophila*-infected cells at 3 to 8 hpi (Figure 3B and 3C). Both proteins became

127 clearly detectable by 24 hpi, showing the highest observed signal intensity at this time point,
128 followed by a reduction to approximately 30% of that level by 48 hpi. To further assess protein
129 expression at early stages, we performed immunofluorescence microscopy. In contrast to
130 Western blot results, WcNdk1 and WcNdk2 signals were already detectable from 0 to 8 hpi,
131 colocalizing with intracellular *W. chondrophila* (Figure S1). Together, these results suggests
132 that both WcNdk paralogs are expressed throughout the developmental cycle, with
133 transcription peaking early. While protein expression begins early, overall accumulation or
134 detection sensitivity peaks around 24 hpi, followed by a decline toward the end of the cycle.

135 **Subcellular localization of WcNdk1 and WcNdk2 in *C. trachomatis* heterologous**
136 **expression**

137 While signal peptides are typically associated with protein secretion, previous studies have
138 demonstrated that Ndk can be secreted in certain bacterial species despite lacking a canonical
139 signal sequence[26–28]. Moreover, the secretion of both WcNdk1 and WcNdk2 into the host cell
140 cytoplasm is experimentally shown[29], suggesting that WcNdk2 signal peptide may not
141 contribute to secretion. The presence of this signal peptide suggests that WcNdk2 may be
142 translocated to a specific subcellular compartment and possibly confers a distinct biological
143 role to WcNdk2 compared to WcNdk1. To assess this possibility, we overexpressed a V5-
144 tagged version of WcNdk1 and WcNdk2 in *C. trachomatis* and studied their subcellular
145 localization by immunofluorescence and confocal microscopy (Figure 4). In this heterologous
146 expression assay, WcNdk1 was exclusively detected inside the inclusion, closely associated
147 with *C. trachomatis*, and no signal was observed in the host cell cytoplasm. Although this does
148 not rule out secretion of WcNdk1, it suggests limited accumulation or detection outside the
149 inclusion. In contrast, WcNdk2 was detected within both chlamydial inclusions and the host-
150 cell nucleus, indicating its trafficking into the nucleus. To further investigate the nuclear
151 localization of WcNdk2, we cloned the gene into the pBOMBL vector[30] and overexpressed the
152 protein in *C. trachomatis*. Upon infection of McCoy cells with the transformed bacteria,
153 inclusions were smaller, and bacterial growth was impaired compared to controls. Due to these
154 growth defects, we could not confirm the nuclear localization of WcNdk2 in this system.

155 **Subcellular localization of WcNdk1 and WcNdk2 in transfected HEK293T cells**

156 To further confirm the observed subcellular localization of WcNdk1 and WcNdk2 in another
157 heterologous system, we transiently expressed the V5-tagged WcNdk1 and WcNdk2 in
158 HEK293T cells and analyzed their distribution by immunofluorescence microscopy. WcNdk1
159 was found exclusively in the cytoplasm absent from cell compartments such as nucleus or

160 Golgi (Figure 5), whereas WcNdk2 showed two mutually exclusive distribution patterns. In
161 some cells the V5 signal was found throughout the nucleus, while in others, it was localized to
162 perinuclear-Golgi regions, with no nuclear signal (Figure 5).

163 **The Ndk inhibitor, Azidothymidine (AZT), inhibits the growth of *W. chondrophila***

164 Since *W. chondrophila* is not currently amenable to genetic modifications, we employed
165 chemicals to inhibit Ndk function in this pathogen. AZT (3′-azido-3′-deoxythymidine), also
166 known as zidovudine, is a known Ndk inhibitor[14,31–35]. This pharmaceutical, primarily
167 approved for the treatment of human immunodeficiency virus (HIV), inhibits viral reverse
168 transcription through chain termination[36]. This compound is structurally a thymidine analogue,
169 where the 3'-hydroxyl group on the deoxyribose sugar is replaced by an azido group (N_3)
170 (Figure 6A).

171 The inhibition of Ndk from *Aspergillus flavus* by AZT is documented, where AZT forms a
172 strong hydrogen bond with key active site residues of Ndk (Arg-104, His-117 and Asp-120)
173 and inhibits its enzymatic activity[14]. Since these residues are highly conserved in Ndks of
174 diverse organisms, including WcNdk1 and WcNdk2, we hypothesized that AZT could also
175 serve as an effective inhibitor of Ndks in *W. chondrophila* (Figure 2A).

176 To test this hypothesis, we treated both uninfected and *W. chondrophila*-infected cells with
177 increasing concentrations of AZT following infection and measured cell lysis resulting from
178 bacterial proliferation using propidium iodide (PI) staining. PI binds to the DNA of lysed cells
179 and is used to assess plasma membrane integrity and cell death. In the absence of AZT or at
180 low concentrations (1 µg/ml) *W. chondrophila*-infected cultures exhibited a sharp increase in
181 cell mortality over time, reaching maximal levels by 144 hpi. Treatment with AZT at
182 concentrations above 25 µg/ml significantly suppressed infection-induced cell death. A delay
183 in cell mortality was observed with the intermediate concentration of 5 µg/ml (Figure 6B, right
184 panel). In contrast, in uninfected cells, cell lysis remained comparable across all AZT
185 concentrations, showing no significant difference from the no-AZT control. Therefore, the
186 slight increase in cell death observed over time is due to normal cell aging and culture
187 dynamics, and not due to the AZT effect (Figure 6B, left panel). These results indicate that
188 AZT did not exhibit adverse effects on mammalian host cells and provided a protective effect
189 against *W. chondrophila*-induced cell death in a dose-dependent manner.

190 **Only early AZT treatment prevents *W. chondrophila*–mediated host cell lysis**

191 To define the temporal window in which AZT exhibits its inhibitory effect on *W. chondrophila*
192 growth, *W. chondrophila*-infected cell monolayers were treated with 25 µg/ml AZT at 0, 3, 8,

193 24, 32, or 48 hpi and the propidium iodide (PI) uptake was monitored at 24, 48, 72, and 144
194 hpi (Figure 6C). When AZT was added at 0, 3, or 8 hpi, cell mortality remained minimum
195 (approximately 25% at 144 hpi), comparable to uninfected controls, indicating complete
196 protection against bacterial-induced lysis. In contrast, administering AZT at 24 hpi or later
197 failed to prevent cell death, resulting in maximum cell lysis, comparable to the no-AZT control.
198 This indicates that once RB replication is well established, AZT cannot reverse the course of
199 infection. Taken together, these results suggest that AZT must be applied before 24 hpi,
200 coinciding with maximum RB replication and inclusion expansion, to fully prevent *W.*
201 *chondrophila*–induced cytotoxicity, whereas later administration results in reduced
202 effectiveness.

203 **AZT induced the production of aberrant bodies (ABs) in *W. chondrophila***

204 To investigate the cellular-level effects of AZT treatment on *W. chondrophila* infection, we
205 performed confocal microscopy on *W. chondrophila*-infected McCoy cells treated with 25
206 µg/ml AZT at 0 hpi. In untreated cultures, *W. chondrophila* underwent normal intracellular
207 development, leading to host cell lysis at the end of infection. At 8 hpi, *W. chondrophila* EBs
208 were observed attached to the host cell surface and internalized in both AZT-treated and
209 untreated cultures indicating that AZT does not interfere with bacterial attachment or entry
210 (Figure 6D). By 24 hpi, inclusions had formed in both conditions. However, in AZT-treated
211 cells, these inclusions failed to expand, and only a limited number of bacteria were detected
212 within them. This suggests that although EB-to-RB differentiation and initial rounds of
213 replication may occur, bacterial proliferation is subsequently arrested. In addition, the *W.*
214 *chondrophila* RBs appeared slightly enlarged in AZT-treated cultures, consistent with the
215 formation of aberrant bodies (ABs). These abnormal conditions persisted until 72 hpi,
216 indicating a disruption of the normal developmental cycle likely resulting in bacterial
217 persistence.

218 **Effect of AZT on *W. chondrophila* growth is probably correlated with WcNdk2 activity**

219 As mentioned earlier, *W. chondrophila* encodes two *ndk* paralogs, organized in single operon
220 with *pabA* positioned in between them. To investigate which Ndk copy mediates susceptibility
221 to AZT, and whether this susceptibility is linked to the presence of the *pabA* gene, we selected
222 representative *Chlamydiota* species with different *ndk* operon configurations and compared
223 their response to AZT treatment. The selected species include *C. trachomatis*, which carries a
224 single *ctndk* gene and lacks *pabA*; *Simkania negevensis,* which also has a single *snndk* gene
225 but retains *pabA* elsewhere in the genome; *Estrella lausannensis*, which harbors a two-gene

226 *elndk1–elndk2* operon without *pabA*; and *W. chondrophila*, which contains the full *wcndk1–*
227 *pabA–wcndk2* operon (Figure 7, bottom panel). To evaluate the effect of AZT on these species,
228 cell monolayers were infected, treated with 25 µg/ml at 0 hpi and fixed at 48 hpi before
229 immunostaining and observation under confocal microscopy. As shown in figure 7, *C.*
230 *trachomatis* and *S. negevensis* exhibited normal intracellular development in presence of AZT,
231 indicating no significant growth inhibition. In contrast, *E. lausannensis*, like *W. chondrophila*,
232 displayed enlarged intracellular structures resembling aberrant bodies. This suggest that AZT
233 inhibitory effect depends on the presence of *ndk2*, regardless of the presence of *ndk1* and *pabA*.

234 DISCUSSION

235 The diversity of *ndk* copy number within members of the *Chlamydiota* phylum reveals lineage-
236 specific adaptations with potential metabolic and pathogenic consequences. While most
237 *Chlamydiales* species possess a single *ndk* gene, a subset, including members of the
238 *Parachlamydiaceae*, *Waddliaceae*, and *Criblamydiaceae*, harbors a second copy (*ndk2*), likely
239 arising from a gene duplication event. The observed gene duplication may have provided a
240 selective advantage by providing increasing metabolism flexibility, which could, in part,
241 account for the comparatively faster growth of *W. chondrophila* and *E. lausannensis* in
242 mammalian cells relative to bacteria of *Chlamydiaceae*. Such an expansion of metabolic
243 capacities might also represent an adaptation facilitating persistence and replication within
244 free-living protists, suggesting that these lineages have evolved mechanisms enabling survival
245 across diverse host environments. This is in line with their larger genome size (>2 Mb),
246 expanded metabolic genes and their reduced dependence on host-derived metabolites. On the
247 other side, the absence of the second copy of the *ndk* gene in *Rhabdochlamydiaceae*,
248 *Simkaniaceae* and *Chlamydiaceae* coincides with their adaptations to more specific host niches
249 and reduced metabolic pathways. The *pabA* gene is also absent in all members of the
250 *Chlamydiaceae* family. In this family, enzymes from other biosynthetic pathways are recruited
251 to meet their folate requirements[37]. The mechanisms driving the evolution of this operon in
252 certain chlamydial families remains unknown. Further studies are needed to clarify the
253 operon's functional role and its evolutionary pathways in these families.

254 Both *W. chondrophila ndk* paralogs retain the universally conserved HGSD active-site motif
255 and surrounding hydrophobic residues essential for autophosphorylation and
256 phosphotransferase activities. This conservation suggests that both Ndk1 and Ndk2, despite

257 their apparent different subcellular localizations, exert their functions, at least partially, through
258 phosphorylation mechanisms.
259 The temporal expression patterns of *wcndk1* and *wcndk2* provide insights into their potential
260 biological roles and regulation during the *W. chondrophila* developmental cycle. The
261 organization of *wcndk1* and *wcndk2* within a single operon explains their synchronized
262 expression profiles. The apparent mid-cycle surge in Ndk proteins at 24 hpi coincides with the
263 maximal bacterial replication, an increased demand for NTPs, and an increased host-
264 manipulation activities that are essential for intracellular growth.
265 Despite sharing conserved kinase domains, our study showed significant differences in
266 subcellular localization of WcNdk1 and WcNdk2. This divergence in their localizations
267 suggests functional specializations and may indicate that the two proteins utilize divergent
268 cellular trafficking mechanisms during *W. chondrophila* infection.
269 In *C. trachomatis* expression system, WcNdk1 was confined to the inclusion. This restricted
270 distribution suggests that WcNdk1 may primarily serve bacterial intracellular functions within
271 the inclusion. It is also possible that WcNdk1 is secreted transiently or at levels insufficient to
272 be detected via immunofluorescence. In contrast, WcNdk2 exhibited nuclear localization both
273 in *C. trachomatis* and HEK293T expression systems. This nuclear localization is consistent
274 with previous studies on other pathogens, where Ndk was shown to bind host DNA and regulate
275 gene expression through DNA cleavage[17,18]. Such putative nuclear activity suggests a potential
276 role for WcNdk2 in reprogramming host transcriptional responses to favor bacterial survival.
277 It would be of great interest to identify the specific host genes targeted by WcNdk2, as this
278 could uncover previously unrecognized mechanisms by which *W. chondrophila* manipulates
279 host cell function and could provide broader insights into its pathogenesis.
280 When expressed in HEK293T cells, WcNdk2 localized not only to the nucleus but also to the
281 perinuclear-Golgi region. Bacterial Ndks, such as *Porphyromonas gingivalis* Ndk, are found
282 in the perinuclear area of the host cells. This localization has been linked to the modulation of
283 host purinergic signaling via $P2X_7$ receptors[28], implying that the perinuclear localization of
284 WcNdk2 could be a biologically relevant phenomenon rather than nonspecific aggregation.
285 Unlike the perinuclear accumulation of bacterial Ndks, Golgi localization represents a novel
286 observation not previously reported for any bacterial species. One plausible explanation for an
287 association of WcNdk2 with the Golgi is that, after translocation into the host cytosol, WcNdk2
288 enters the classical ER–Golgi secretory pathway and is packaged into Golgi-derived vesicles
289 for extracellular release to hydrolyze host extracellular ATP (eATP) and subvert purinergic

290 signaling. Another possible explanation for the Golgi recruitment of WcNdk2 is that it might
291 play a role in modulating vesicle trafficking between the Golgi and the bacterial inclusion.
292 Although *W. chondrophila* does not redirect sphingomyelin transport from the Golgi to its
293 inclusion[38], it may still influence other aspects of vesicular trafficking, altering vesicle
294 formation or fusion processes, to benefit bacterial survival or replication.
295 AZT is a well-established inhibitor of Ndk[14,31–35]. In our study, AZT treatment of *W.*
296 *chondrophila*-infected cells protected them from bacteria-induced cell lysis and bacterial
297 growth was arrested in the replication phase. Our comparative data across *Chlamydiales*
298 species suggest that WcNdk2 is most likely the target for AZT. The inhibition of WcNdk2 by
299 AZT appears to interfere with a function that is essential for bacterial survival. Our results
300 demonstrated that WcNdk2 localizes to host cell compartments, including the nucleus,
301 perinuclear region, and Golgi apparatus in a heterologous expression system. Such host-
302 directed localization implies that secretion of WcNdk2 facilitates its accessibility to AZT and
303 may be critical for its effector functions within the host cell. Thus, bacterial growth arrest may
304 result from a disruption of Ndk2-dependent pathogenic mechanisms required for successful
305 replication, proliferation and host-cell manipulation. In contrast, WcNdk1, which
306 predominantly localizes within the inclusion, and is more likely involved in maintaining
307 bacterial nucleotide pools, appears less susceptible to AZT, possibly due to limited drug access
308 to the inclusion compartment. These findings collectively support a model in which the
309 inhibition of host-targeted, secreted WcNdk2, rather than inclusion-confined WcNdk1, is
310 central to AZT's antimicrobial activity against *W. chondrophila*.
311 Based on these observations, we propose a functional model for the two *W. chondrophila* Ndks,
312 as illustrated in Figure 8. Together, these findings highlight multifunctional nature of Ndk
313 proteins and shed light on the distinct roles of *W. chondrophila* Ndks. However, the lack of
314 genetic manipulation tools in *W. chondrophila* currently impedes direct investigation of Ndk
315 function via gene deletion or mutagenesis. Although localization studies using heterologous
316 expression systems suggest that WcNdk2 may interact with host cells, the possibility of
317 overexpression artifacts or mis-localization cannot be entirely ruled out. Additionally, although
318 AZT is a well-established Ndk inhibitor with no other known bacterial targets, direct in vitro
319 evidence confirming WcNdk2 as the AZT target is still missing. In vitro ATPase assays are
320 essential to validate this interaction. In the absence of such studies the proposed functions
321 remain speculative. The advancement of genetic tools would be essential to validate the
322 proposed roles of WcNdk1 and WcNdk2 in *W. chondrophila* metabolism and host interaction.

323 # CONCLUSION

324 Given its diverse activities, Ndk has attracted interest across multiple disciplines, including
325 microbiology, cell biology, and drug development. In this study, we introduced chlamydial Ndk
326 as a multifunctional protein with roles extending beyond nucleotide metabolism, highlighting
327 its potential involvement in host–pathogen interactions. These findings not only enhance our
328 understanding of Ndk biology in the *Chlamydiota* phylum but also point to Ndk2 as a potential
329 therapeutic target, opening new avenues for dissecting host manipulation strategies in obligate
330 intracellular bacteria.

331 # MATERIALS AND METHODS

332 **Phylogenetic and structural analysis**

333 Species-based and *ndk* gene phylogenies were retrieved from the *Chlamydia* Database[39]. Trees
334 were trimmed using FigTree (v1.4.4) to retain only relevant *Chlamydiales* species. The Ndk
335 protein sequences across different taxa were retrieved from the National Center for
336 Biotechnology Information (NCBI). The Multiple sequence alignment of Ndk proteins across
337 eukaryotes and prokaryotes was generated using the ClustalW tool on UGENE and the results
338 were visualized with EPSript https://espript.ibcp.fr/ESPript/cgi-bin/ESPript.cgi. The 3D
339 structure of the protein was reconstructed using Phyre2[40] and visualized using Jmol v.16.2.15.

340 **Cell culture and *W.chondrophila* infection**

341 McCoy and HEK293T cells were maintained at 37°C in 5% CO_2 in DMEM GlutaMAX
342 (Gibco), supplemented with 10% fetal bovine serum (FBS; Gibco). *W. chondrophila* was
343 propagated in *Acanthamoeba castellanii* at 25°C. At the time of infection, lysed *W.*
344 *chondrophila*-infected amoebae were filtered through a 5 mm syringe filter (Life science) to
345 remove amoebal debris. The bacterial solution was then used to infect the host cells at a dilution
346 of 1:1000, which was optimum for infection. To synchronize the infection, the infected cells
347 were centrifuged at 1790 x g for 10 minutes. They were then incubated at 37°C in 5% CO_2 for
348 15 minutes. Following incubation, the inoculum was then replaced with fresh medium.

349 **Purification of recombinant His-tagged WcNdk1 and WcNdk2 for antiserum production**

350 The *E. coli* strain BL21 containing pET28a-*wcndk1-6xHis* or pET28a-*wcndk2-6xHis* was
351 grown to an OD_{600} of 0.5. The culture was induced using 1 mM Isopropyl β-D-
352 thiogalactopyranoside (IPTG, Applichem) and incubated at 37°C for 4 hours to express the
353 recombinant protein. Bacterial pellets were resuspended in native lysis buffer (50 mM

354 NaH_2PO_4, 300 mM NaCl, and 10 mM imidazole, pH 8). The resuspended cells were lysed
355 using a combination of methods: three cycles of freeze (ethanol-dry ice bath) and thaw (at
356 37°C), followed by chemical lysis with 1 mg/ml lysozyme and sonication. The recombinant
357 protein was purified under native condition using Ni-NTA agarose beads (Qiagen) according
358 to the manufacturer's instructions. Briefly, bacterial lysates were incubated with Ni-NTA resin
359 for 2 hours at 4 °C with gentle rotation. The protein-bound resin was then loaded onto poly-
360 prep chromatography columns (Bio-Rad Laboratories), washed with wash buffer (50 mM Tris-
361 HCl, 300 mM NaCl, 20 mM imidazole, pH 8.0), and eluted with elution buffer containing
362 250 mM imidazole. The purified protein was dialyzed using Slide-A-Lyzer Dialysis Cassette
363 (Thermo scientific, 2,000 MWCO) overnight against PBS to remove imidazole. The
364 concentration of the protein was determined using Bradford's reagent with BSA (Bio-Rad
365 Laboratories) as a standard. Following protein purification, antisera were produced using
366 immunization services offered by Eurogentec SA (Seraing, Belgium).

367 **Western Blot**

368 McCoy cells were seeded at a density of 1 x 10^6 per T-25 flask one day before infection and
369 infected with *W. chondrophila* as described above. Infected cells were harvested by scraping at
370 the specified hpi and a fraction of the culture was saved for extraction and quantification of the
371 genomic DNA (see below). The cell suspension was pelleted at 1790 x g for 10 minutes, then
372 washed twice with PBS, and finally resuspended in 0.5 ml of 1x Laemmli sample buffer. An
373 equal volume of each lysate was resolved on 12% SDS-PAGE precast gels (Bio-Rad
374 Laboratories) and transferred onto an Amersham Protran nitrocellulose membrane (Cytiva).
375 The membrane was blocked in saturation buffer (10 mM Tris-Base, 150 mM NaCl, and 0.05%
376 Tween 20) containing 5% nonfat dried milk (AppliChem) for 2 hours at room temperature
377 (RT). Blots were probed overnight at 4°C with primary antibodies diluted in saturation buffer
378 with 0.5% non-fat dried milk. After three washes with saturation buffer containing 0.5% non-
379 fat dried milk, blots were incubated with secondary antibodies (horseradish peroxidase-
380 conjugated anti-rabbit IgG; Promega, or anti-mouse IgG; Bio-Rad Laboratories) for 1 hour at
381 Room temperature and processed using the Amersham ECL detection system (GE Healthcare).
382 Western blot bands intensities were quantified using EvolutionCapt edge x64 software and
383 normalized to the corresponding bacterial genome copy number. Graphs were generated using
384 GraphPad v. 10.4.1.

385 **Extraction of genomic DNA and quantification of *W. chondrophila* genome copy number**

386 Genomic DNA from collected samples was extracted using the Wizard SV Genomic DNA
387 purification system (Promega) according to the manufacturer's instructions. The extracted
388 DNA served as a template for qPCR with iTaq Universal Probes Supermix (Bio-Rad
389 Laboratories) to quantify the *W. chondrophila* bacterial population in 1 µl of culture. The 16S
390 copy numbers were determined using a standard curve, which was generated from serial
391 dilutions of a plasmid containing one copy of the 16S rRNA gene.

392 **RNA extraction and cDNA synthesis**

393 *W. chondrophila*-infected McCoy cell monolayers or uninfected control cells were harvested
394 at indicated hpi by scraping and centrifugation (5000 x g, 10 minutes). Following
395 centrifugation cells were lysed directly in TRIzol Reagent (Invitrogen). Total RNA was
396 extracted by chloroform separation and recovery of the aqueous phase (12,000 × g, 15 min,
397 4 °C). RNA was precipitated with isopropanol, washed with 75 % ethanol, air-dried, and
398 resuspended in RNase-free water. To remove genomic DNA, samples were treated with
399 RNase-free DNase I (Invitrogen) following the manufacturer's instructions. cDNA was
400 synthesized using the GoScript Reverse Transcription System (Promega) with random primers.
401 Reverse transcription was performed at 42°C for 60 minutes, followed by enzyme inactivation
402 at 70°C for 15 minutes. All cDNAs were diluted 1:5 prior to qPCR.

403 **RT-qPCR**

404 The qPCR reactions were set up in a final volume of 20 µl containing 4 µl of cDNA template,
405 the appropriate concentration of each primer, and 1X iTaq Universal SYBR Green Supermix
406 (Bio-Rad Laboratories). All samples were run in duplicates, and no-template controls were
407 included for each primer pair to assess non-specific amplification. The fluorescent reporter
408 signal was normalized against the internal reference dye (ROX) signal. qPCR was carried out
409 on QuantStudio 3 (Applied Biosystems) using the following thermal program. A single cycle
410 of DNA polymerase activation for 3 min at 95 °C, followed by 45 amplification cycles of 15 s
411 at 95 °C (denaturing step) and 1 min at 60 °C (annealing and extension step). Gene expression
412 data were normalized to *W. chondrophila* 16 rRNA gene, which served as the internal reference
413 gene. Quantitative data from qRT-PCR experiments were collected from at least three
414 independent replicates. The primers used for RT-qPCR are listed in Table S1.

415 **Application of AZT on *W. chondrophila* culture and cell death assessment**

416 McCoy cells were seeded at a density of 1×10^4 cells per well in 96-well plates (Corning).
417 Cells were infected with *W. chondrophila* or left uninfected as a control. To monitor cell lysis,

418 Propidium Iodide (PI, 7 µg/mL, Sigma-Aldrich) was added to the growth medium. AZT was
419 purchased from TOCRIS (Cat. No.:4150) and was added to the wells at concentrations ranging
420 from 0 to 250 µg/mL in six technical replicates per condition. Depending on the experimental
421 design, AZT was added at the time of infection (0 hpi) or at later time points (3, 8, 24, 32, and
422 48 hpi). PI fluorescence was measured at specified time points post-infection using a FLUOstar
423 Omega plate reader (BMG LABTECH; excitation: 540 nm; emission: 640 nm). To define
424 100% cell lysis, 0.1% Triton X-100 was added to control wells prior to PI reading.

425 **Immunofluorescence assay**

426 McCoy cells were cultured on glass coverslips placed in 24-well-plates and infected with
427 various bacterial species. At the indicated time points, cells were fixed with ice-cold methanol
428 for 5 minutes at 4°C, followed by three washes with phosphate-buffered saline (PBS). Fixed
429 cells were permeabilized and blocked for 30 minutes using a blocking solution containing
430 0.1% saponin, 10% fetal bovine serum (FBS), and 0.04% sodium azide in PBS. Blocked cells
431 were incubated with primary antibodies for 2 hours at RT. After three washing steps with
432 blocking solution, cells were incubated for 1 hour with Alexa Fluor 488-conjugated secondary
433 antibodies (Invitrogen, 1:1000 dilution) to stain bacteria. DAPI (Invitrogen, 1:3000 dilution)
434 and Texas Red-conjugated Concanavalin A (Invitrogen) were used to stain nuclei and
435 carbohydrates, respectively. Cells were then washed three times with PBS and briefly rinsed
436 with purified water before mounting. Coverslips were mounted on glass slides with Mowiol 4-
437 88 and stored in the dark until imaging using Zeiss LSM 900 confocal laser scanning
438 microscope (Carl Zeiss Microscopy GmbH).

439 **pGL2 plasmid construction**

440 The genes *wcndk1* and *wcndk2* were amplified from *W. chondrophila* genomic DNA using
441 primers with 5′ overhangs compatible with the pGL2 backbone. All PCR products included a
442 C-terminal V5 epitope tag to facilitate detection. PCR products were purified using the
443 QIAquick PCR Purification Kit (Qiagen). The native *C. trachomatis*–derived pGL2 vector
444 (11,786 bp; β-lactamase selection marker) was linearized by Age I digestion (NEB) and
445 recovered from agarose gels with the QIAquick Gel Extraction Kit (Qiagen). Purified inserts
446 and linearized vector were assembled via In-fusion cloning using 5X In-fusion Snap assembly
447 Master Mix (Takara). Assemblies were incubated at 50 °C for 15 min. Transformations were
448 performed using *E. coli* dam^- dcm^- cells. Transformants were selected on LBA supplemented
449 with Carbenicillin (50 µg/mL). Positive clones were screened by colony PCR, and successful
450 insertions were confirmed by Sanger sequencing using both vector- and insert-specific primers.

451 ***C. trachomatis* transformation**

452 Transformation of *C. trachomatis* was performed with minor modifications to previously
453 described methods[41].1 x 10^6 McCoy cells were seeded in 6-well plates and cultured overnight.
454 2.5 x 10^6 plasmid-free *C. trachomatis* serovar L2 was incubated with 2 µg of sequence-verified
455 plasmid DNA for 30 minutes. The quantity of plasmid-free *C. trachomatis* serovar L2 (EBs),
456 resuspended in 300µl Tris-$CaCl_2$ buffer (10 mM Tris, 50 mM CaCl2, pH 7.4), and incubated
457 with 2 µg of sequence-verified plasmid DNA for 30 minutes. 1 mL Hank's balanced salt
458 solution (HBSS, Gibco) was then added to each reaction. This mixture was added to McCoy
459 cells in a 6-well plate after removing the medium. The infection was carried out by
460 centrifugation at 400 × g for 15 minutes at room temperature and incubation at 37°C for 15
461 minutes. Then, the inoculum was removed, and cells were incubated with 2 mL of DMEM
462 medium supplemented with 10% FBS and 1 µg/mL cycloheximide for 8 hours at 37°C and 5%
463 CO_2. After this incubation, the medium was replaced with DMEM containing 10% FBS, 1
464 µg/mL cycloheximide, and penicillin (0.6 mg/mL) to select for transformed bacteria. Cells
465 were passaged every 48 hours, and the development of fluorescent inclusions were monitored
466 until they were clearly observed and established. The transformed *C. trachomatis* was
467 harvested and titrated by IFU assay and stored at -80°C. For experiments requiring induction,
468 50 ng/ml anhydrotetracycline (aTc, Sigma-Aldrich) was added at the time of infection,
469 whereas, in control conditions, the inducer was excluded.

470 **Gateway cloning for mammalian expression in pDEST47**

471 For generation of pDEST47 expression plasmids, attB-flanked primers were used to amplify
472 the C-terminal V5-tagged version of *wcndk1* and *wcndk2*. Entry clones were created by BP
473 recombination (Gateway BP Clonase, Invitrogen), following the manufacturer's protocol. The
474 resulting pDONR201-*ndk-V5* entry clones were selected on appropriate antibiotic. Destination
475 vectors were generated via LR recombination of the entry clones with pDEST47 using LR
476 Clonase (Gateway, Invitrogen), according to the supplier's instructions. Final constructs were
477 transformed and validated as described above, with plasmid DNA prepared from overnight
478 cultures using the GeneJET plasmid Miniprep kit (Thermo Scientific).

479 **Transfection in HEK293T cells**

480 Glass coverslips in 24-well plates were coated with poly-L-lysine (Sigma-Aldrich) at a final
481 concentration of 100 µg/ml, incubated for 30 minutes at room temperature, washed three times
482 with PBS, and air-dried for 3 hours. HEK293T cells were then seeded on coated coverslips at
483 2×10^5 cells per well and incubated overnight at 37 °C, 5% CO_2. HEK293T cells were

484 transfected 24 hours post-seeding with the pDEST47 plasmids using the lipofectamine 3000
485 transfection kit (Invitrogen). DNA (3 μg) was diluted in 150 μL serum-free DMEM with 6 μL
486 P3000 reagent. Separately, 4.5 μL Lipofectamine 3000 (Invitrogen) was diluted in 150 μL
487 DMEM. The two mixtures were combined, incubated for 15 minutes at room temperature, and
488 50 μL was added dropwise per well. Cells were fixed 24 hours post-transfection with ice-cold
489 methanol for downstream immunofluorescence analysis.

FIGURES

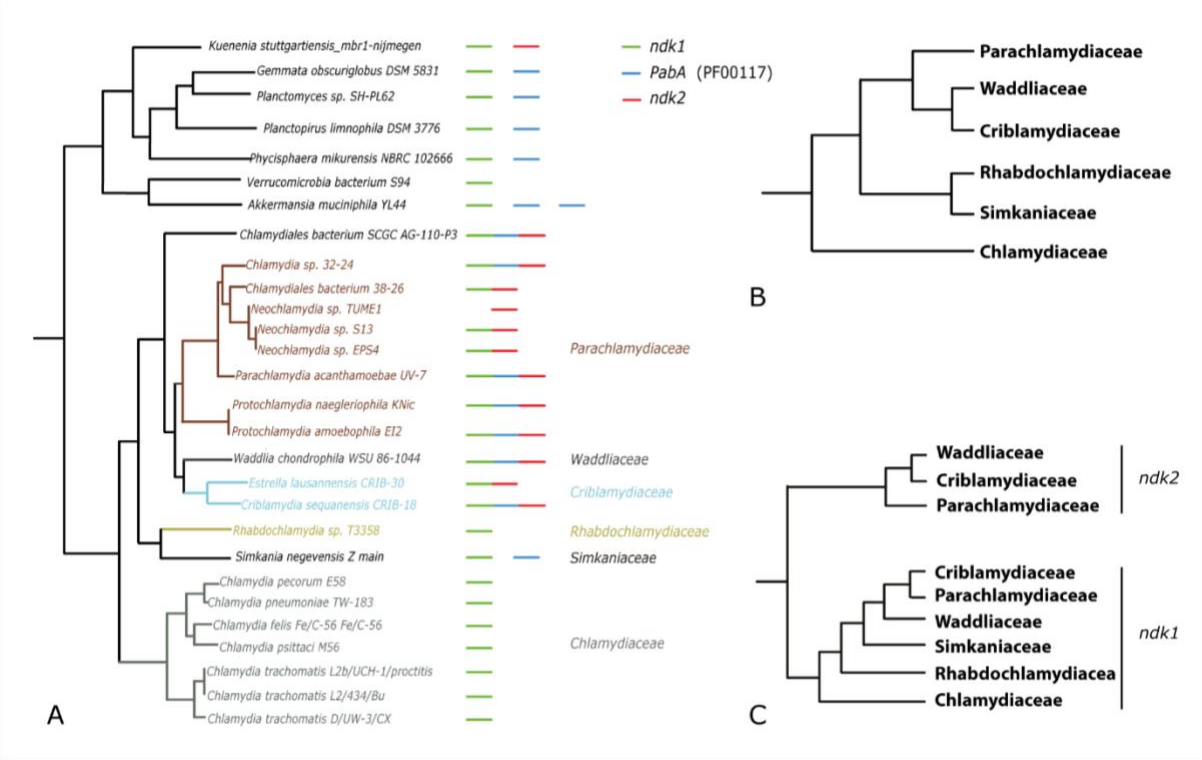

Figure1: Phylogeny of *Chlamydiota* phylum and the *ndk* gene operon evolution. (A) Species phylogeny based on 32 single-copy orthologous genes. (B) Simplified representation of the species phylogeny highlighting major clades. (C) Phylogeny based on the *ndk* gene, showing its evolutionary relationship among *Chlamydiales* species.

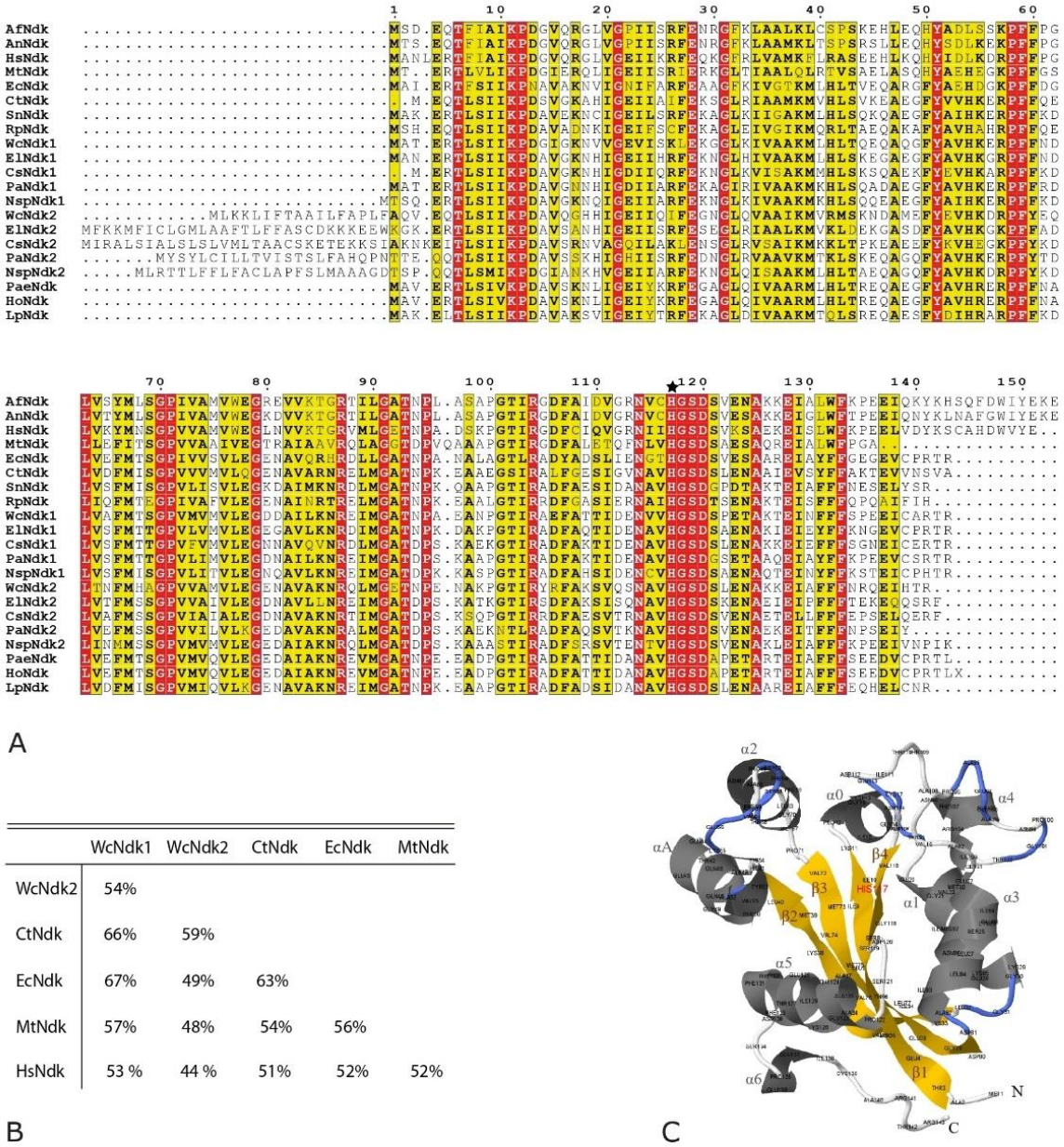

Figure 2: Ndk sequence and structure conservation. (A) Multiple sequence alignment of Ndk proteins across eukaryotes and prokaryotes, generated using ClustalW tool on UGENE and visualized with https://espript.ibcp.fr/ESPript/cgi-bin/ESPript.cgi. Conserved residues are highlighted in red with the highly conserved H residue, essential for catalytic activity, marked with an asterisk. Af: *Aspergillus flavus*, An: *A. niger*, Hs: *Homo sapiens*, Mt: *Mycobacterium tuberculosis*, Ec: *Escherichia coli,* Ct: *C. trachomatis*, Sn: *Simkania negevensis*, Rp: *Rhabdochlamydia porcellionis,* Wc: *W. chondrophila*, El: *Estrella lausannensis,* Cs: *Criblamydia sequanensis,* Pa: *Parachlamydia acanthamoebae,* Nsp: *Neochlamydia sp.*, Pae: *Pseudomonas aeruginosa*, Ho: *Halofilum ochraceum*, Lp: *Legionella pneumophila* (B) Amino acid sequence similarity matrix comparing Ndk proteins from *W. chondrophila* (WcNdk1 and WcNdk2), *Chlamydia trachomatis* (CtNdk), *Escherichia coli* (EcNdk), *Mycobacterium tuberculosis* (MtNdk), and human Ndk (HsNdk). (C) Predicted 3D structure of WcNdk1, illustrating its conserved α/β fold characteristic of the Ndk family. 3D structure reconstructed using Phyre2 and visualized using Jmol v.16.2.15. The H177, highlighted in red, is a critical histidine residue and positioned within the active site.

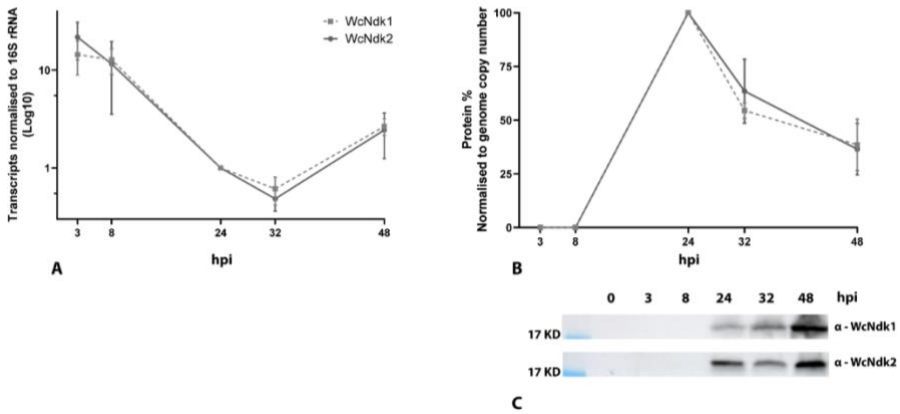

Figure 3: Temporal expression analysis of *ndk* paralogs in *W. chondrophila* during infection. (A) Quantitative RT-PCR analysis of *ndk1* and *ndk2* transcript levels at different hours post-infection (hpi), normalized to 16S rRNA. Transcript abundance is expressed relative to the 24 hpi time point, which was set as the reference (1.0). (B) Relative protein levels of WcNdk1 and WcNdk2 quantified by Western blot, normalized to bacterial genome copy number. Protein expression is shown relative to 24 hpi, set as 100%. (C) Representative Western blot images showing WcNdk1 and WcNdk2 expression across the infection time course. Data are shown as mean ± SD of 3 independent experiments.

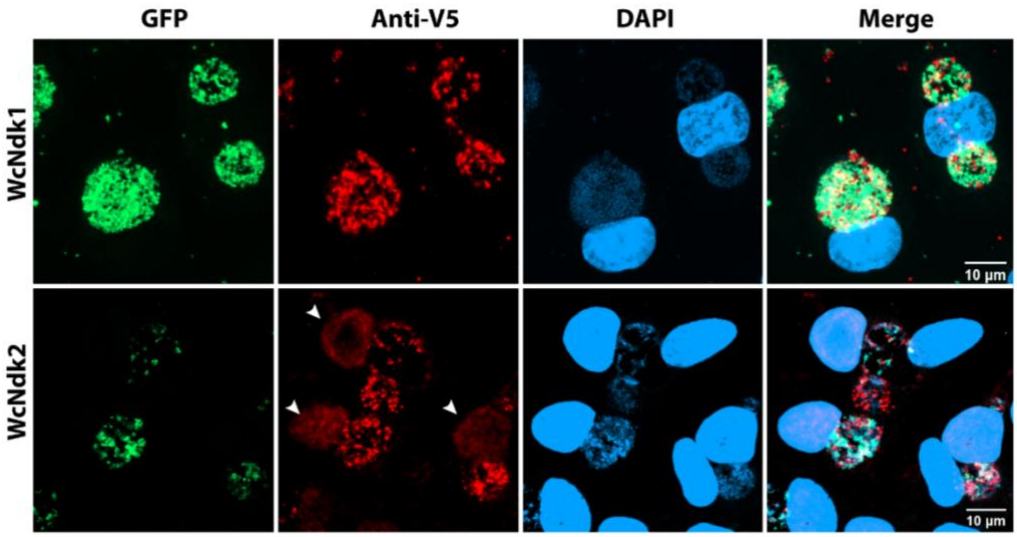

Figure 4: Subcellular localization of WcNdk1 and WcNdk2 overexpressed in *C. trachomatis*. *C. trachomatis* was transformed with plasmids expressing either WcNdk1 or WcNdk2 tagged with a V5 epitope. Infected McCoy cells were fixed at 24 hpi. GFP (green) indicates transformed *C. trachomatis*, anti-V5 (red) detects WcNdk proteins, and DAPI (blue) stains host cell nuclei and bacterial DNA. White arrows point to V5 signal within host nuclei.

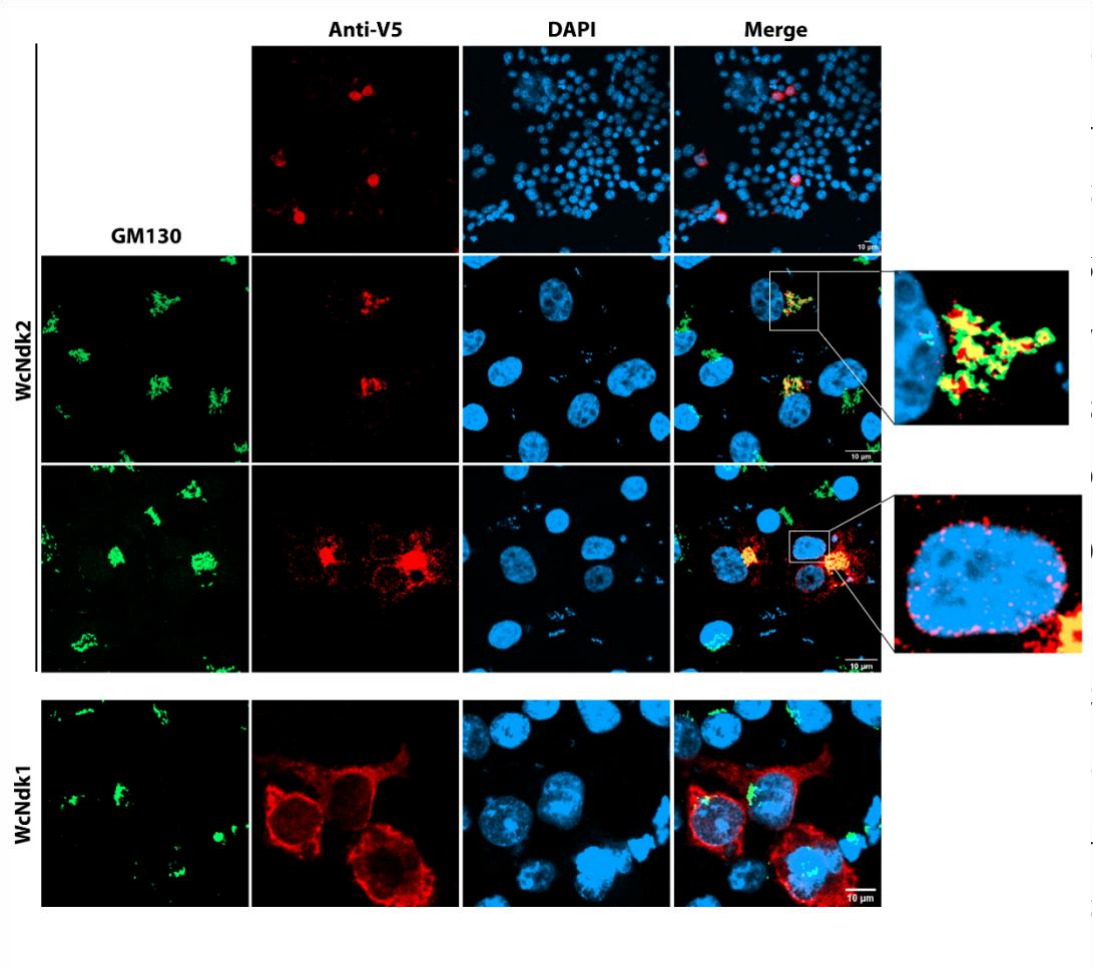

Figure 5: Subcellular distribution of WcNdk1 and WcNdk2 in HEK293T Cells. HEK293T cells were transiently transfected with C-terminal V5-tagged WcNdk1 and WcNdk2 and stained with the Golgi marker GM130 (green), anti-V5 antibody (red), and DNA (DAPI, blue). High-magnification insets highlight the co-localization of WcNdk2 (red) with the Golgi (green) or the perinuclear region.

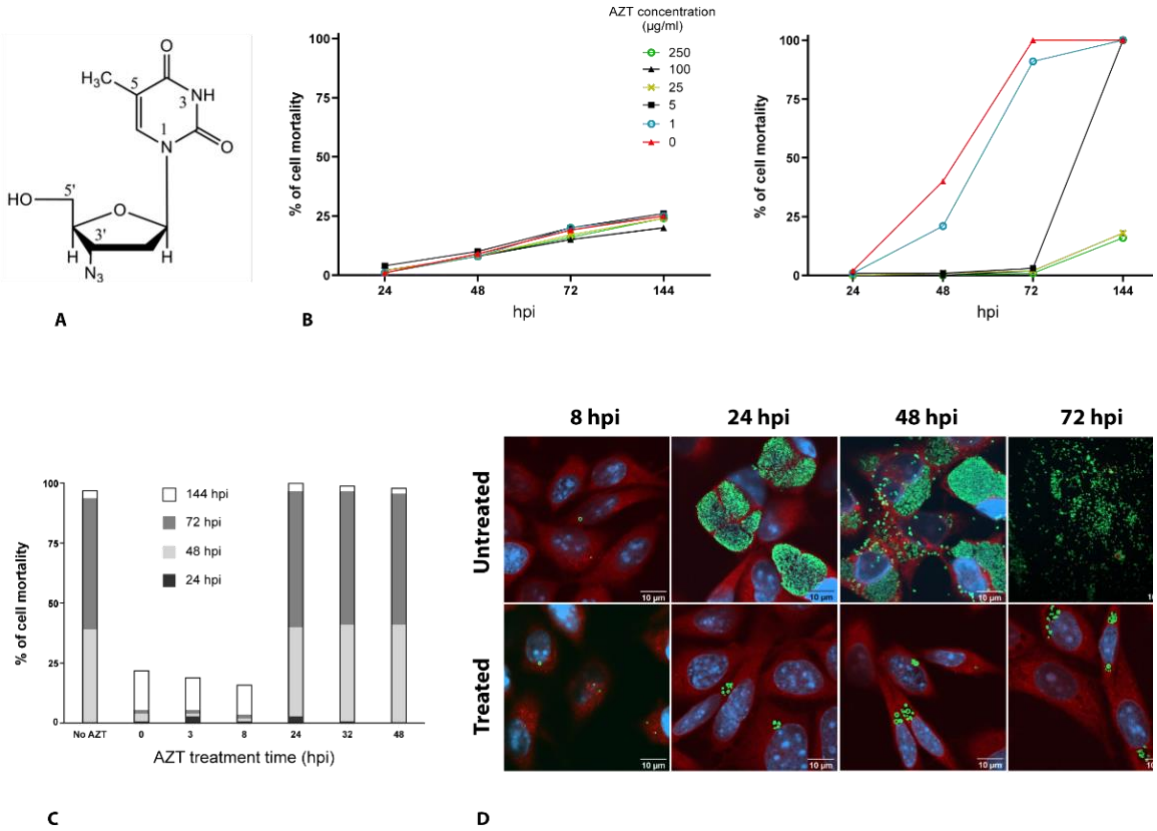

Figure 6: AZT inhibits *W. chondrophila* growth in infected host cells. (A) Chemical structure of azidothymidine (AZT). (B) AZT treatment of uninfected host cells, serving as a negative control (left panel) and treatment of infected host cells at concentrations ≥25 µg/mL (right panel). (C) Effect of AZT addition on *W. chondrophila*-infected cultures at various time points after infection. (D) Confocal microscopy of *W. chondrophila*-infected cells treated or not treated with AZT. In untreated conditions, *W. chondrophila* formed typical intracellular inclusions, whereas AZT treatment resulted in enlarged, aberrant structures. Bacteria are labeled using anti-*W. chondrophila* antibody (green); host cell nuclei are stained with DAPI (blue); and the host structures are marked with Concanavalin A (red).

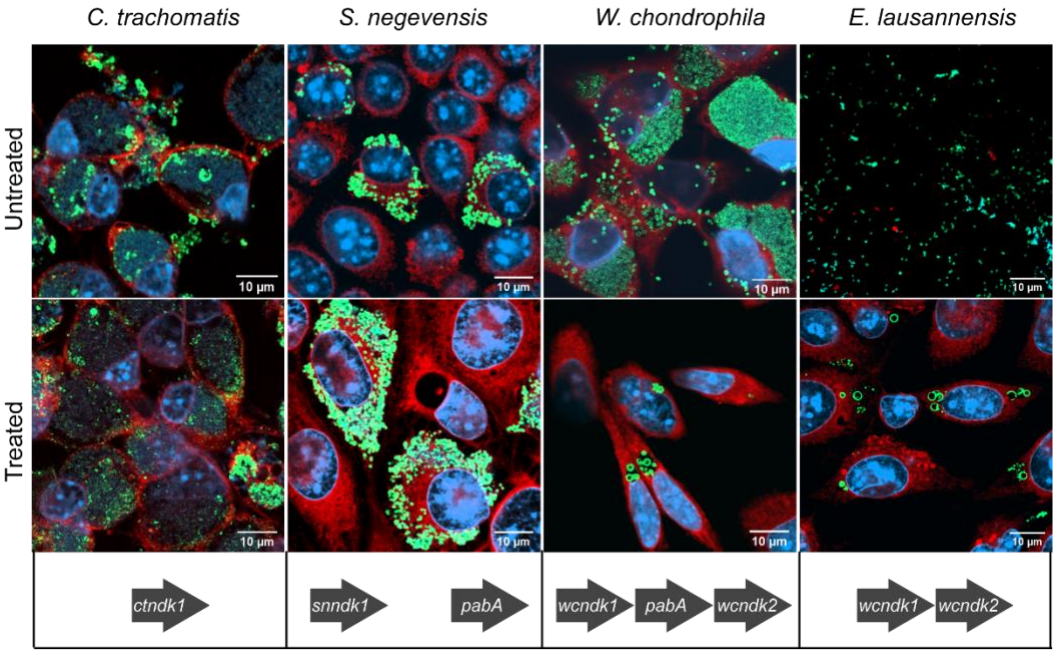

Figure 7: AZT sensitivity is restricted to *Chlamydiales* species encoding *ndk2*. Representative confocal micrographs of McCoy cells infected with *C. trachomatis*, *S. negevensis*, *W. chondrophila* or *E. lausannensis*, treated or not treated with 25 µg/ml AZT. The infected cells were fixed and stained 48 hpi. The lower panel shows the *ndk* operon arrangement: *C. trachomatis* and *S. negevensis*, each carries a single *ndk* gene. *S. negevensis* retains *pabA* elsewhere in the genome. *W. chondrophila* carries the two *ndk* genes with a *pabA* in the middle. *E. lausannensis* encodes a two-gene *ndk1–ndk2* operon but lacks *pabA*. Bacteria are stained in green using species-specific antibodies, host cytoplasm is labeled with Concanavalin A (red), and nuclei are stained with DAPI (blue). *ctndk*: *C. trachomatis ndk1*, *snndk1*: *S. negevensis ndk1*, *elndk1*: *E. lausannensis ndk1*, *elndk2*: *E. lausannensis ndk2.*

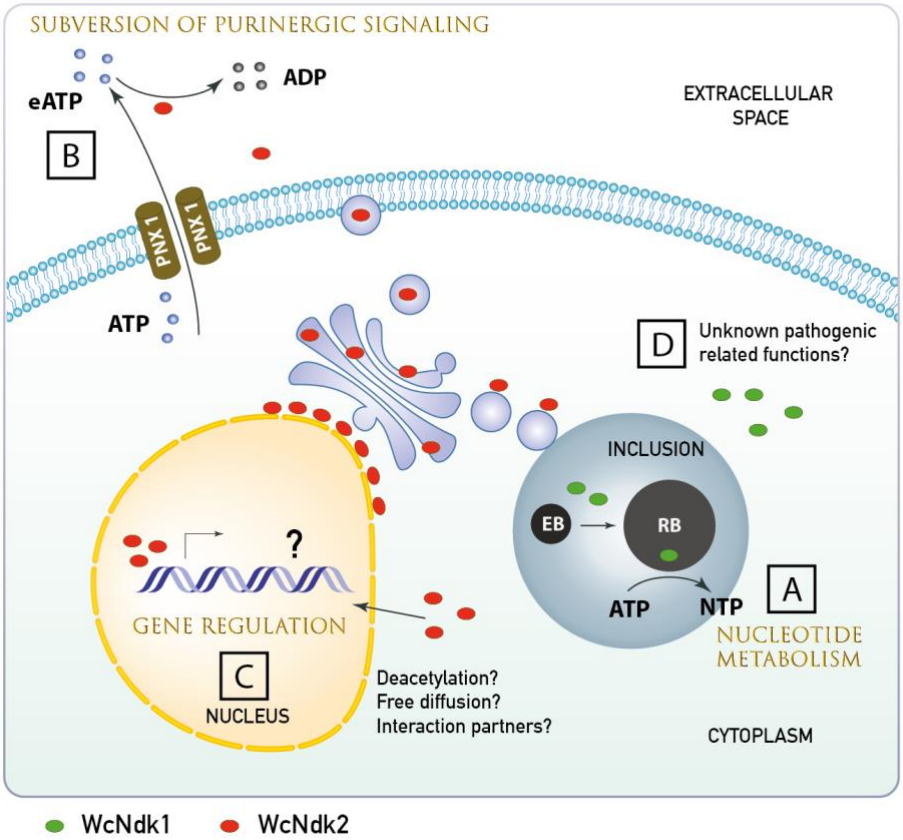

Figure 8: Proposed model for WcNdk1 and WcNdk2 functions in *W. chondrophila.* This schematic illustrates the distinct subcellular localizations and putative roles of WcNdk1 (green) and WcNdk2 (red), during infection of a host cell. A: WcNdk1 is predominantly retained within the bacterial inclusion, where it sustains basic nucleotide metabolism and "housekeeping" functions. B: A fraction of WcNdk1 is secreted across the inclusion membrane into the host cytosol, however, the specific functions of cytosolic WcNdk1 remain undefined. C: WcNdk2 is observed accumulating within the host nucleus. Its import into the nucleus could occur via one or more of the following mechanisms: a deacetylation event allowing passive nuclear import; free diffusion through nuclear pores owing to its small molecular size; or interaction with host proteins that escort WcNdk2 into the nucleus. Inside host nucleus, WcNdk2 could bind directly to DNA leading to up- or downregulation of host genes involved in immunity or apoptosis. The precise gene targets remain unknown. D: WcNdk2 traffics through Golgi/ER-derived vesicles and perinuclear region. This localization may be related to the packaging of WcNdk2 into vesicles destined for secretion to subvert host purinergic signaling through hydrolyzes of eATP into ADP. E: The association of WcNdk2 with Golgi apparatus implies its involvement in vesicle trafficking and acquisition of host-derived metabolites necessary for expansion of the inclusion and bacterial survival.

FUNDING

This work was supported by the Swiss National Science Foundation (SNSF) [Grant No. 197768].

REFERENCES

1. Dilbeck PM, Evermann JF, Crawford TB, et al. Isolation of a previously undescribed rickettsia from an aborted bovine fetus. *J Clin Microbiol*. 1990;28(4):814-816
2. Henning K, Schares G, Granzow H, et al. *Neospora caninum* and *Waddlia chondrophila* strain 2032/99 in a septic stillborn calf. *Veterinary Microbiology*. 2002;85(3):285-292. doi:10.1016/S0378-1135(01)00510-7
3. Dilbeck-Robertson P, McAllister MM, Bradway D, Evermann JF. Results of a new serologic test suggest an association of *Waddlia chondrophila* with bovine abortion. *J Vet Diagn Invest*. 2003;15(6):568-569. doi:10.1177/104063870301500609
4. Baud D, Thomas V, Arafa A, Regan L, Greub G. *Waddlia chondrophila*, a Potential Agent of Human Fetal Death. *Emerg Infect Dis*. 2007;13(8):1239-1243. doi:10.3201/eid1308.070315
5. Baud D, Goy G, Osterheld MC, Borel N, Vial Y, pospischil A, Greub G. *Waddlia chondrophila*: from bovine abortion to human miscarriage. *Clin Infect Dis*. 2011;52(12):1469-1471. doi:10.1093/cid/cir205
6. Baud D, Regan L, Greub G. Emerging role of Chlamydia and Chlamydia-like organisms in adverse pregnancy outcomes. *Curr Opin Infect Dis*. 2008;21(1):70-76. doi:10.1097/QCO.0b013e3282f3e6a5
7. Haider S, Collingro A, Walochnik J, Wagner M, Horn M. Chlamydia-like bacteria in respiratory samples of community-acquired pneumonia patients. *FEMS Microbiol Lett*. 2008;281(2):198-202. doi:10.1111/j.1574-6968.2008.01099.x
8. Goy G, Croxatto A, Posfay-Barbe KM, Gervaix A, Greub G. Development of a real-time PCR for the specific detection of *Waddlia chondrophila* in clinical samples. *Eur J Clin Microbiol Infect Dis*. 2009;28(12):1483-1486. doi:10.1007/s10096-009-0804-7
9. de Barsy M, Greub G. *Waddlia chondrophila*: from biology to pathogenicity. *Microbes and Infection*. 2013;15(14):1033-1041. doi:10.1016/j.micinf.2013.09.010
10. K Kebbi-Beghdadi C, Cisse O, Greub G. Permissivity of Vero cells, human pneumocytes and human endometrial cells to *Waddlia chondrophila*. *Microbes and Infection*. 2011;13(6):566-574. doi:10.1016/j.micinf.2011.01.020

537 11. Scherler A, Jacquier N, Kebbi-Beghdadi C, Greub G. Diverse Stress-Inducing Treatments cause
538 Distinct Aberrant Body Morphologies in the Chlamydia-Related Bacterium, *Waddlia*
539 *chondrophila*. *Microorganisms*. 2020;8(1):89. doi:10.3390/microorganisms8010089
540 12. Timmons L, Shearn A. Role of AWD/Nucleoside Diphosphate Kinase in Drosophila Development.
541 *J Bioenerg Biomembr*. 2000;32(3):293-300. doi:10.1023/A:1005545214937
542 13. Masoudi N, Fancsalszky L, Pourkarimi E, et al. The NM23-H1/H2 homolog NDK-1 is required for
543 full activation of Ras signaling in C. elegans. *Development*. 2013;140(16):3486-3495.
544 doi:10.1242/dev.094011
545 14. Wang Y, Wang S, Nie X, et al. Molecular and structural basis of nucleoside diphosphate kinase–
546 mediated regulation of spore and sclerotia development in the fungus Aspergillus flavus. *J Biol*
547 *Chem*. 2019;294(33):12415-12431. doi:10.1074/jbc.RA119.007505
548 15. Muñoz-Dorado J, Inouye S, Inouye M. Nucleoside diphosphate kinase from Myxococcus xanthus.
549 II. Biochemical characterization. *Journal of Biological Chemistry*. 1990;265(5):2707-2712.
550 doi:10.1016/S0021-9258(19)39859-X
551 16. Postel EH, Berberich SJ, Rooney JW, Kaetzel DM. Human NM23/Nucleoside Diphosphate Kinase
552 Regulates Gene Expression through DNA Binding to Nuclease-Hypersensitive Transcriptional
553 Elements. Published online 2000:8.
554 17. Levit MN, Abramczyk BM, Stock JB, Postel EH. Interactions between Escherichia coli nucleoside-
555 diphosphate kinase and DNA. *J Biol Chem*. 2002;277(7):5163-5167. doi:10.1074/jbc.M11117020
556 18. Kumar P, Verma A, Saini AK, et al. Nucleoside diphosphate kinase from Mycobacterium
557 tuberculosis cleaves single strand DNA within the human c-myc promoter in an enzyme-catalyzed
558 reaction. *Nucleic Acids Res*. 2005;33(8):2707-2714. doi:10.1093/nar/gki568
559 19. Coutinho-Silva R, Ojcius DM. Role of extracellular nucleotides in the immune response against
560 intracellular bacteria and protozoan parasites. *Microbes Infect*. 2012;14(14):1271-1277.
561 doi:10.1016/j.micinf.2012.05.009
562 20. Kolli BK, Kostal J, Zaborina O, Chakrabarty AM, Chang KP. *Leishmania*-released nucleoside
563 diphosphate kinase prevents ATP-mediated cytolysis of macrophages. *Molecular and Biochemical*
564 *Parasitology*. 2008;158(2):163-175. doi:10.1016/j.molbiopara.2007.12.010
565 21. Yilmaz Ö, Yao L, Maeda K, et al. ATP scavenging by the intracellular pathogen Porphyromonas
566 gingivalis inhibits P2X7-mediated host-cell apoptosis. *Cellular Microbiology*. 2008;10(4):863-
567 875. doi:10.1111/j.1462-5822.2007.01089.x
568 22. Ardissone S, Scherler A, Pillonel T, Martin V, Kebbi-Beghdadi C, Greub G. Transcriptional
569 Landscape of *Waddlia chondrophila* Aberrant Bodies Induced by Iron Starvation. *Microorganisms*.
570 2020;8(12):1848. doi:10.3390/microorganisms8121848
571 23. Arumugam M, Ajitkumar P. Histidine 117 in the His-Gly-Ser-Asp motif is Required for the
572 Biochemical Activities of Nucleoside Diphosphate Kinase of Mycobacterium smegmatis. *Open*
573 *Biochem J*. 2012;6:71-77. doi:10.2174/1874091X01206010071

574 24. Singh S, Yadav PK, Singh AK. In-silico structural characterization and phylogenetic analysis of
575 Nucleoside diphosphate kinase: A novel antiapoptotic protein of Porphyromonas gingivalis.
576 *Journal of Cellular Biochemistry*. 2023;124(4):545-556. doi:10.1002/jcb.30389
577 25. Janin J, Dumas C, Moréra S, et al. Three-Dimensional Structure of Nucleoside Diphosphate Kinase.
578 *J Bioenerg Biomembr*. 2000;32(3):215-225. doi:10.1023/A:1005528811303
579 26. Kamath S, Chen ML, Chakrabarty AM. Secretion of Nucleoside Diphosphate Kinase by Mucoid
580 Pseudomonas aeruginosa 8821: Involvement of a Carboxy-Terminal Motif in Secretion. *J*
581 *Bacteriol*. 2000;182(13):3826-3831.
582 27. Neeld D, Jin Y, Bichsel C, et al. Pseudomonas aeruginosa injects NDK into host cells through a
583 type III secretion system. *Microbiology (Reading)*. 2014;160(Pt 7):1417-1426.
584 doi:10.1099/mic.0.078139-0
585 28. Atanasova K, Lee J, Roberts J, Lee K, Ojcius DM, Yilmaz Ö. Nucleoside-Diphosphate-Kinase of
586 P. gingivalis is Secreted from Epithelial Cells In the Absence of a Leader Sequence Through a
587 Pannexin-1 Interactome. *Scientific Reports*. 2016;6(1). doi:10.1038/srep37643
588 29. Kebbi-Beghdadi C, Pilloux L, Martin V, Greub G. Eukaryotic Cell Permeabilisation to Identify
589 New Putative Chlamydial Type III Secretion System Effectors Secreted within Host Cell
590 Cytoplasm. *Microorganisms*. 2020;8(3):361. doi:10.3390/microorganisms8030361
591 30. Ouellette, S. P., Blay, E. A., Hatch, N. D. & Fisher-Marvin, L. A. CRISPR Interference To Inducibly
592 Repress Gene Expression in Chlamydia trachomatis. Infect Immun 89, e00108-21. doi:
593 10.1128/IAI.00108-21
594 31. Valenti D, Barile M, Quagliariello E, Passarella S. Inhibition of nucleoside diphosphate kinase in
595 rat liver mitochondria by added 3′-azido-3′-deoxythymidine. *FEBS Letters*. 1999;444(2-3):291-
596 295. doi:10.1016/S0014-5793(99)00071-X
597 32. Schaertl S, Konrad M, Geeves MA. Substrate Specificity of Human Nucleoside-diphosphate
598 Kinase Revealed by Transient Kinetic Analysis. *Journal of Biological Chemistry*.
599 1998;273(10):5662-5669. doi:10.1074/jbc.273.10.5662
600 33. Gallois-Montbrun S, Schneider B, Chen Y, et al. Improving Nucleoside Diphosphate Kinase for
601 Antiviral Nucleotide Analogs Activation. *Journal of Biological Chemistry*. 2002;277(42):39953-
602 39959. doi:10.1074/jbc.M206360200
603 34. Xu Y, Sellam O, Moréra S, et al. X-ray analysis of azido-thymidine diphosphate binding to
604 nucleoside diphosphate kinase. *Proceedings of the National Academy of Sciences*.
605 1997;94(14):7162-7165. doi:10.1073/pnas.94.14.7162
606 35. Wambaugh MA, Shakya VPS, Lewis AJ, Mulvey MA, Brown JCS. High-throughput identification
607 and rational design of synergistic small-molecule pairs for combating and bypassing antibiotic
608 resistance. *PLOS Biology*. 2017;15(6):e2001644. doi:10.1371/journal.pbio.2001644
609 36. Furman PA, Barry DW. Spectrum of antiviral activity and mechanism of action of zidovudine. An
610 overview. *Am J Med*. 1988;85(2A):176-181.

611 37. Adams NE, Thiaville JJ, Proestos J, et al. Promiscuous and Adaptable Enzymes Fill "Holes" in the
612 Tetrahydrofolate Pathway in Chlamydia Species. *mBio*. 2014;5(4):e01378-14.
613 doi:10.1128/mBio.01378-14
614 38. Dille S, Kleinschnitz EM, Kontchou CW, Nölke T, Häcker G. In contrast to *Chlamydia trachomatis*,
615 *Waddlia chondrophila* grows in human cells without inhibiting apoptosis, fragmenting the Golgi
616 apparatus, or diverting post-Golgi sphingomyelin transport. *Infect Immun*. 2015;83(8):3268-3280.
617 doi:10.1128/IAI.00322-15
618 39. Pillonel T, Tagini F, Bertelli C, Greub G. ChlamDB: a comparative genomics database of the
619 phylum Chlamydiae and other members of the Planctomycetes-Verrucomicrobiae-Chlamydiae
620 superphylum. *Nucleic Acids Research*. 2020;48(D1):D526-D534. doi:10.1093/nar/gkz924
621 40. Kelley LA, Mezulis S, Yates CM, Wass MN, Sternberg MJE. The Phyre2 web portal for protein
622 modeling, prediction and analysis. *Nat Protoc*. 2015;10(6):845-858. doi:10.1038/nprot.2015.053
623 41. Mueller KE, Wolf K, Fields KA. *Chlamydia trachomatis* transformation and allelic exchange
624 mutagenesis. *Curr Protoc Microbiol*. 2017;45:11A.3.1-11A.3.15. doi:10.1002/cpmc.31
625